Materials Transactions, Vol. 49, No. 4 (2008) pp. 704 to 709

Parallel Computer Simulation of Three-Dimensional Grain Growth Using the Multi-Phase-Field Model

Yoshihiro Suwa[1], Yoshiyuki Saito[2] and Hidehiro Onodera[3]

[1]*Computational Materials Science Center, National Institute for Materials Science, Tsukuba 305-0047, Japan*
[2]*Department of Materials Science and Engineering, Waseda University, Tokyo 169-8555, Japan*
[3]*Materials Engineering Laboratory, National Institute for Materials Science, Tsukuba 305-0047, Japan*

We have performed computer simulations of normal grain growth in three-dimension by using the multi-phase-field (MPF) model. For the purpose of the acceleration of computation, we have applied both the active parameter tracking algorithm and parallel coding techniques to the MPF model. The simulation results have been compared with those obtained in previous simulations and a theoretical treatment. We have reconfirmed that the MPF is a powerful tool for simulating grain growth. Especially, the procedure described in this paper is highly efficient. [doi:10.2320/matertrans.MRA2007225]

(Received September 25, 2007; Accepted January 11, 2008; Published February 20, 2008)

Keywords: *computer simulation, parallel computation, phase field modeling, grain growth*

1. Introduction

Modeling of kinetics of grain growth is essentially important for designing structural materials. Due to the difficulty of incorporating topological features into analytical theories of grain growth directly[1–5] there has been increasing interest in the use of computer simulations to study grain growth.[6–19] Recently, the phase-field models[14–19] have been widely applied to simulating grain growth. Furthermore, in order to reduce their enormous computational cost, which has been the main drawback of multi orientation field models,[14–18] a number of algorithms have been proposed.[18,20–24] Especially, Kim *et al.*[18] applied highly efficient algorithm to the multi phase-field (MPF) model proposed by Steinbach *et al.*,[25] and justified Hillert's mean field approximation[3] in 3D normal grain growth. It is well known that, in normal grain growth, an invariant distribution of scaled grain sizes develops in its steady state. Further, the grain growth obeys a power law kinetics with a characteristic exponent of $1/2$.[26] Thus, the larger system size and the longer simulation time are preferable to verify whether simulated microstructures truly reach the steady state.

In this study, we reconfirm the applicability of the MPF to the simulations of grain growth. The simulation results will be compared with those obtained in previous simulations and a theoretical treatment, especially the results in Ref. 21) that were obtained by Fan and Chen model[14,15] coupled with dynamic grain-orientation reassignment (DGR) algorithm[20–22] and parallel computation techniques. We apply both the active parameter tracking (APT) algorithm[23] and parallel coding techniques to the MPF model to accelerate computations and to embody large scale calculations.

2. Method

2.1 Phase-field model

To represent the temporal evolution of polycrystalline material we utilize the multi phase-field (MPF) model. In this study, a set of continuous field variables, $\phi_1(\boldsymbol{r}, t)$, $\phi_2(\boldsymbol{r}, t), \ldots, \phi_N(\boldsymbol{r}, t)$, is defined to distinguish the orientation of grains, where $\phi_i(\boldsymbol{r}, t)$ represents the existence ratio of each orientation at a position $\boldsymbol{r}$ and a time t. As described later, in order to avoid coalescence between grains having the same field number, i, we apply each different number to each different grain (*i.e.* $N-1$ is assumed to be the total number of grains in an initial microstructure). Here we outline the equations from the MPF model, which are essential for simulating grain growth. Details of the model were described in Ref. 25), 27), 28):

The sum of each phase-field at any position in the system is conserved.

$$\sum_{i=1}^{N} \phi_i(\boldsymbol{r}, t) = 1. \tag{1}$$

The evolution equation of the phase-field is given by

$$\frac{\partial \phi_i}{\partial t} = -\frac{2}{n(\boldsymbol{r}, t)} \sum_{j \neq i}^{N} s_i s_j M_\phi \left[\frac{\delta F}{\delta \phi_i} - \frac{\delta F}{\delta \phi_j} \right], \tag{2}$$

where M_ϕ is the isotropic phase-field mobility and

$$\frac{\delta F}{\delta \phi_i} = \sum_{j \neq i}^{N} \left[\frac{\epsilon^2}{2} \nabla^2 \phi_j + \omega \phi_j \right] + f_i^E, \tag{3}$$

where ϵ is the gradient energy coefficient and ω is the height of the parabolic potential with a double obstacle, assumed to be isotropic; f_i^E is the excess free energy for the each orientation, assumed to be constant. The number of phases coexisting in a given point, $n(\boldsymbol{r}, t)$, can be written as

$$n(\boldsymbol{r}, t) = \sum_{i=1}^{N} s_i(\boldsymbol{r}, t), \tag{4}$$

where $s_i(\boldsymbol{r}, t)$ is a step function which satisfies $s_i(\boldsymbol{r}, t) = 1$ if $\phi_i > 0$ and $s_i(\boldsymbol{r}, t) = 0$ otherwise.

For the purpose of numerical simulation, the set of phase-field eq. (2) has to be solved numerically by discretizing them in space and time. The second-order central difference method and the simple explicit Euler equation are used for discretization with respect to space and time, respectively.

2.2 Active parameter tracking algorithm

In the MPF model, in order to perform simulations with

avoiding the coalescence between grains which have the same field number, a number of algorithms have been proposed.[18,20–24)]

More recently, Vedantam and Patnaik[23)] have devised an efficient new algorithm called active parameter tracking (APT) algorithm for solving MPF equations numerically. Gruber *et al.*[24)] and Kim *et al.*[18)] also devised essentially the same algorithm. In the MPF model, at every grid point, only a few field variables are nonzero and they contribute toward the evolution of grains; these nonzero variables are referred to as active field variables. In the APT algorithm, we only consider the evolution of the active field variables at each grid point instead of all the N variables. In this study, we apply both the APT algorithm and parallel coding techniques to the MPF model. The parallelization of the APT algorithm is fairly easy as compared to that of the DGR algorithm. The only requirement is that the data arrays located along the surfaces of each adjacent message-passing interface (MPI) domain communicate with each other at every time step.

The number of active field variables is used as the value of $n(\boldsymbol{r}, t)$. Because the total amount of memory consumption is approximately proportional to the maximum number of $n(\boldsymbol{r}, t)$—n_{max}, we apply following procedures depending on the value of $n(\boldsymbol{r}, t)$ in order to reduce the value of n_{max}:

If $n(\boldsymbol{r}, t) < n_{max}$; we introduce the threshold value, ϕ_{th}, for $\{\phi_i(\boldsymbol{r}, t)\}(i = 1 \ldots N)$. Further, if the value of $\phi_i(\boldsymbol{r}, t)$ becomes smaller than that of ϕ_{th}, ϕ_i is forced to be inactive at the position $\boldsymbol{r}$ and the time t. The value of ϕ_{th} is set to be 1.0×10^{-40}.

If $n(\boldsymbol{r}, t) = n_{max}$; the active field variable, ϕ_i, which has the smallest value among the active field variables is forced to be inactive at the position $\boldsymbol{r}$ and the time t.

The value of n_{max} was determined from preliminary computation as $n_{max} = 6$. Note that the condition described by eq. (1) is updated at the end of each time step for all grid points. Before the operation, the values $\phi_i(\boldsymbol{r}, t) \leq 0$ and $\phi_i(\boldsymbol{r}, t) \geq 1$ are cut off. In the case of the simulation of the normal grain growth, the memory consumption was 1/3 of that in Ref. 21) (Fan and Chen model with the DGR algorithm and the parallel coding techniques). The difference will be larger with the introduction of anisotropy into grain boundary properties.

2.3 Model parameters and simulation procedure

All calculations are performed on 3D lattice with periodic boundary conditions. The target materials are not specified in this paper. However, in order to express simulation results in actual units such as [s] and [m], physical properties are assumed as follows: The phase-field mobility is set to be $M_\phi = 4.0 \times 7/6 \times 10^{-8} \approx 4.67 \times 10^{-8}[\mathrm{m^3 J^{-1} s^{-1}}]$. It is assumed to be a constant value in a simulation run. The physical grain boundary mobility is calculated to be $M_p = 2.27 \times 10^{-14}[\mathrm{m^4 J^{-1} s^{-1}}]$ by using other physical properties described in this section.[18,27)] The value of grain boundary energy is $\sigma = 1.0[\mathrm{J/m^2}]$. The lattice step size Δx is set to be 1.0×10^{-7}[m] and the boundary width, 2ξ, is assumed to be $6.0 \times \Delta x$.

Hereafter, length and volume are expressed in [m] and [$\mathrm{m^3}$], respectively. Then the parameters ϵ and ω are calculated as $\epsilon = 4/\pi(3\Delta x\sigma)^{0.5}$ and $\omega = 2\sigma/3\Delta x$, respectively.[27)] We also perform simulations with the condition $2\xi = 7.0 \times \Delta x$ to evaluate the effects of the boundary width. In this case, the value of M_ϕ is set to be $M_\phi = 4.0 \times 10^{-8}[\mathrm{m^3 J^{-1} s^{-1}}]$ in order not to change the value of M_p. A step for time integration, Δt of 6.5×10^{-2}[s] is employed. The system size of $(5.12 \times 10^{-5})^3$ (134217728 grid points) is employed throughout this paper.

The initial microstructure for computation are obtained by putting spherical grains on the randomly sampled positions in the system with a constant excess free energy, $f_1^E > 0$; the excess free energy for the spherical grains is set to be $f_i^E = 0 (i = 2, \ldots, 50001)$. The number of grain embedded in the system is 50000. All calculations in this paper have been performed on the Numerical Materials Simulator (HITACHI SR11000) at National Institute for Materials Science (NIMS) with 2 nodes (number of central processing units: $16 \times 2 = 32$, memory for application codes: $24 \times 2 = 48$ GB). The computation for 260[s]($4000\Delta t$) required approximately 10 hours and 24 hours for 650[s]($10000\Delta t$).

3. Results and Discussion

In order to get statistical values such as grain size and grain face distributions, three runs of simulation were performed with the boundary width condition $2\xi = 6.0 \times \Delta x$. And only a run of simulation was performed with the condition, $2\xi = 7.0 \times \Delta x$. The computational time became smaller with a dcrease in the boundary width especially in the early stage of simulation. However, the effect of boundary width on the computaional time became smaller with a decrease in the number of grains. It is attributed to a decrease in the boundary regions only at which the computation of eq. (2) is required. Hereafter, we mainly refer to the results with the boundary condition $2\xi = 6.0 \times \Delta x$.

The temporal evolutions of microstructure with the boundary width condition $2\xi = 6.0 \times \Delta x$ is shown in Fig. 1. The number of grains in the system, N_g, is 35174 at $t = 32.5$[s]($500\Delta t$) and 1185 at $t = 650$[s]($10000\Delta t$). In order to analyze simulated microstructures we have tried both the methods utilized in Ref. 21)) (*i.e.*, cluster enumeration) and that utilized in Ref. 18)) (*i.e.*, simple summation); in Ref. 21), a function $O(\boldsymbol{r}, t)$ was defined to perform cluster enumeration[29)] as follows: When $\phi_q(\boldsymbol{r}, t)$ had the maximum value among all field variable at a lattice point, $\boldsymbol{r}$, $O(\boldsymbol{r}, t)$ was set to be the variable number, q. On the other hand, in Ref. 18), the volume of the grain with a field variable name was obtained by simply summing up all the values of the variable with the name without cluster enumeration; this easiness of the calculating topological characteristics of grains is an advantage of MPF+APT scheme. As expected, the number of grain estimated by the simple summation has become larger. However, the difference in the estimation has been negligibly small. For example, the difference in the number of grain at $t = 650$[s] was only two. Thus, we have mainly used the cluster enumeration; the simple summation was used for only obtaining Fig. 5.

The square of average grain radius, $\langle r \rangle^2$, versus simulation time is shown in Fig. 2, where we have defined the value of $\langle r \rangle$ as $\langle r \rangle = \langle (3v_i/4\pi)^{1/3} \rangle$ and v_i is the volume of each grain. The value of $\langle r \rangle^2$ is found to be proportional to simulation

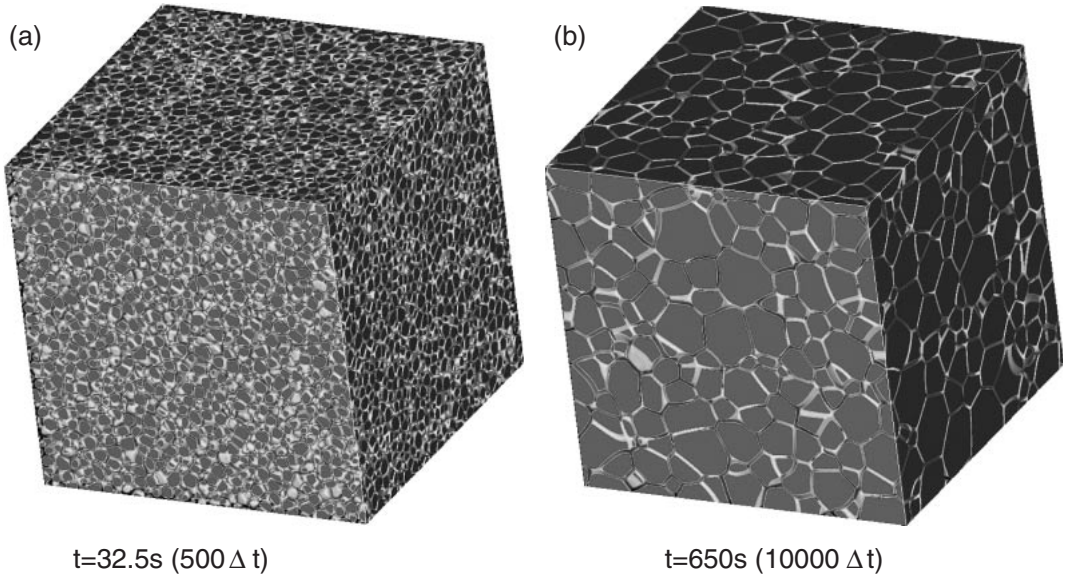

Fig. 1 Simulated microstructural evolution in 512^3 cells; (a) 35174 grains at $t = 32.5$[s] and (b) 1185 grains at $t = 650$[s]. All microstructures in this figure were obatined with the boundary width condition $2\xi = 6.0 \times \Delta x$.

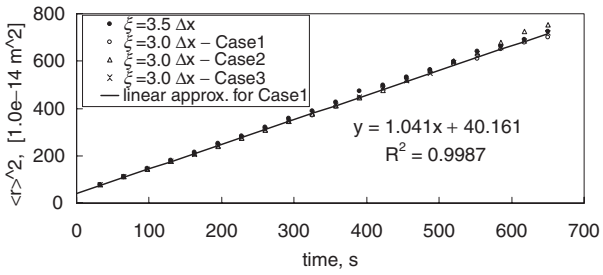

Fig. 2 The square of average grain radius, $\langle r \rangle^2$, versus simulation time. The thick straight line is the linear least-square fitting for a simulation run ($2\xi = 6.0 \times \Delta x$-Case1, $t \geq 65$[s]).

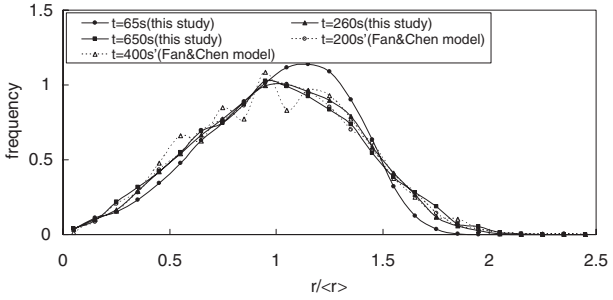

Fig. 3 Evolution of the grain size distribution (GSD) during the 3D normal grain growth. For comparison, we also plot the GSD that were obtained in Ref. 21)) normalized by $\langle r \rangle$ instead of $\langle r' \rangle$.

time. The kinetic coefficient k is obtained as $k = 1.04 \times 1.0^{-14}$ (for $2\xi = 6.0 \times \Delta x$-Case1) by a least-squares fitting.

Next, the grain size distributions (GSDs) normalized by the value of $\langle r \rangle$ are plotted in Fig. 3. In Ref. 21), we defined the average grain radius as $\langle r' \rangle = (3V_{\text{all}}/4\pi N_g)^{1/3}$, where V_{all} was the volume of the system. However, the value of $\langle r' \rangle$ is not always identical to the value of $\langle r \rangle$ if the distribution has a finite width. Therefore, we also plot the GSDs those were obtained in Ref. 21) normalized by $\langle r \rangle$ instead of $\langle r' \rangle$. In this

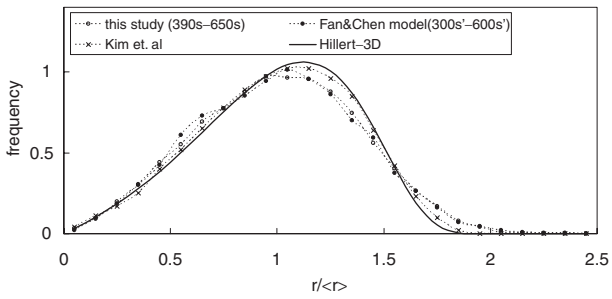

Fig. 4 The steady-state grain size distributions from various phase-field simulations of the 3D normal grain growth; Suwa *et al.*[21] (Fan and Chen model+DGR), Kim *et al.*[18] (MPF model, symbols were taken from Fig. 15 in Ref. 18)) and this study (MPF model+APT algorithm). The thick curve depicts the 3D distribution predicted by Hillert theory.[3]

figure, s' represents the dimensionless time used in Ref. 21). Except for the distribution at $t = 65$ s, the shape of GSDs is very similar, although the distribution at $t = 400\,s'$ (8000*step*) is highly fluctuated due to an insufficient number of grains.

We compare the GSD from this study with those from previous phase-field simulations and a mean field treatment. Figure 4 shows the distributions from phase-field simulation by Suwa *et al.*[21] (Fan and Chen model+DGR), Kim *et al.*[18] (MPF model, symbols were taken from Fig. 15 in Ref. 18)) and this study (MPF model+APT algorithm), where curve drawn by the thick line is the 3D distribution from the Hiller theory.[3] Although Fan and Chen model was utilized in Ref. 21) these two GSDs look very similar. Compared with GSD from Kim *et al.*, the GSD from this study is symmetric and slightly broader. The model and simulation condition in Ref. 18) is almost identical to those in this study. One possible cause of the dissimilar distributions is the difference in the simulation time. In this study, the time required to reach steady state is around 390[s](5000Δt). Note that the achievement to the steady state is judged by the microstructural entropy, *Me*,[30] and the second moment of face

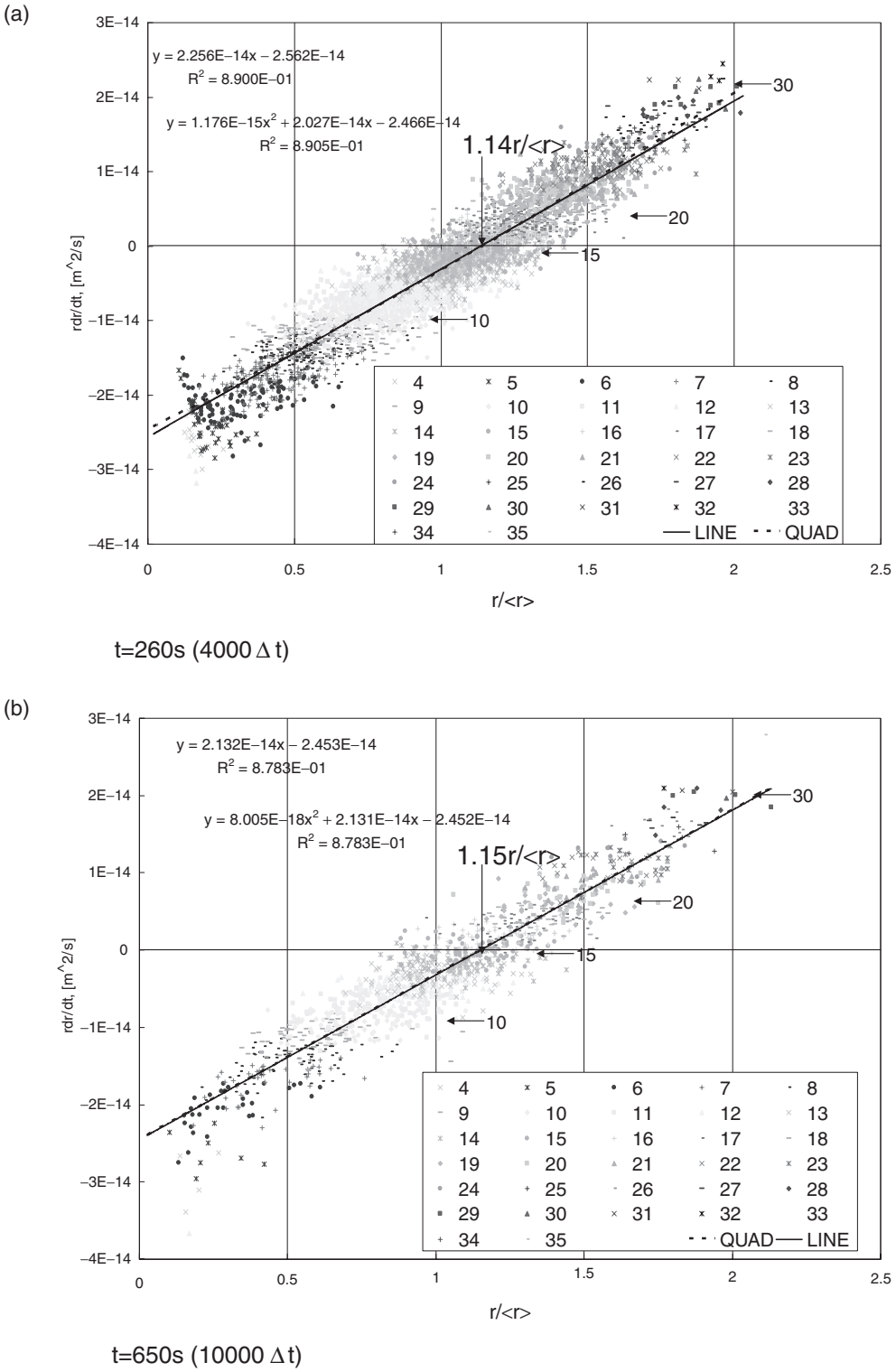

Fig. 5 Simulation test of mean-field approximation [eq. (5)] in the 3D normal grain growth. The results obtained from a simulation run ($2\xi = 6.0 \times \Delta x$-Case1) at (a) $t = 260$[s] and (b) $t = 650$[s] are shown in this figure, where 4165 grains and 1185 grains are shown as dots in a rdr/dt vs $r/\langle r\rangle$ plane. The dr/dt values were measured from the volume changes during a single time step. The thick straight and dashed line are the least-square fitting into a linear (LINE) and a quadratic polynomials (QUAD), respectively.

distribution function, μ_2[31] because they take a constant value at the steady state. We also note that the step for time integration in this study corresponds to 98.3% of the step in Ref. 18) if we represent the step in the same unit. The microstructural entropy of these distributions are calculated as 2.74 (this study), 2.75 (Suwa *et al.*), 2.69 (Kim *et al.*) and 2.66 (Hillert theory).

In Hillert theory,[3] the growth rate of each grain is approximated by the mean-field treatment as

$$\frac{dr}{dt} = \alpha M_p \sigma \left(\frac{1}{r_c} - \frac{1}{r}\right); \quad r\frac{dr}{dt} = \alpha M_p \sigma \left(\frac{r}{r_c} - 1\right), \quad (5)$$

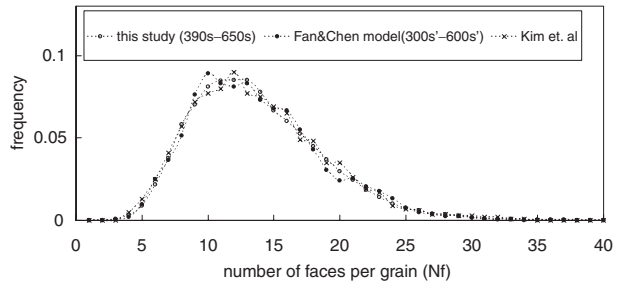

Fig. 6 Distributions of grains with the number of faces per grain in the 3D simulations; Suwa *et al.*[21] (Fan and Chen model+DGR), Kim *et al.*[18] (MPF model, symbols were taken from Fig. 16 in Ref. 18))) and this study (MPF model+APT algorithm).

where r_c is the critical grain radius to be determined later. And α is a constant of the order of unity which represents the approximations inherent in the assumed idealized geometry of the model. Kim *et al.*[18] validated the mean-field eq. (5) by plotting rdr/dt values of grains against $r/\langle r\rangle$. According to Kim *et al.*, the results obtained from the simulation (for $2\xi = 6.0 \times \Delta x$-Case1) at (a) $t = 260$[s] and (b) $t = 650$[s] are shown in Fig. 5, where 4165 grains and 1185 grains are shown as dots in a rdr/dt vs $r/\langle r\rangle$ plane. The dr/dt values were measured from the volume changes during a single time step. The distributions of the dots in Fig. 5-(a),(b) can be well represented by a straight line which is the linear least-square fitting over all the points appearing in the each figure.

In these figures, we can define the critical radius, r_c, as the point of intersection for $rdr/dt = 0$ and the fitting line. They are obtained as $1.14r/\langle r\rangle$ and $1.15r/\langle r\rangle$ for $t = 260$[s] and 650[s], respectively. They are very close to the value $9/8r/\langle r\rangle = 1.125r/\langle r\rangle$ predicted by Hillert theory and obtained in Ref. 18)). When we define the value of r_c as described above, we can also obtain the value of $\alpha M_p\sigma$ as the intercept for rdr/dt axis. Thus, they are 2.56×10^{-14}[m^2/s] and 2.45×10^{-14}[m^2/s] for $t = 260$[s] and 650[s], respectively. Although they may include other than geometric factor such as computation errors, the values of α are estimated as 1.13 and 1.08. In Fig. 5, the least-square fitting into a quadratic polynomial is also plotted as a dashed line.[32,33]

Next, we refer to the face distribution related results. The average face number shows the value of 14.0 at $t =$ 32.5 s[$500\Delta t$]. It decreases with simulation time and approaches to a constant value of 13.7 at around $t = 325$ s[$5000\Delta t$]. The grain distribution with the number of faces per grain in Fig. 6, where the results from the phase-field simulation by Suwa *et al.* (Fan and Chen model+DGR), Kim *et al.* (MPF model, symbols were taken from Fig. 16 in Ref. 18)) and this study (MPF model+APT algorithm) are compared. Although the face number at which the distributions have a maximum value is slightly different, they are almost identical. Finally, we consider the relationship between the average number of faces of per grain adjacent to an N-faced grain, $m(N_f)$, and the face number in grains, N_f, at $t = 390$[$6000\Delta t$] (for $2\xi = 6.0 \times \Delta x$-Case1). The linear relation similar to the Aboav-Weaire relations[34,35] is calculated between $m(n)$ and N_f by the linear least-square fitting for simulation results as $m(N_f) \times N_f = 13.6N_f + 27.2$. The relation is very close to those of $m(N_f) \times N_f = 13.7N_f + 24.7$ and $m(N_f) \times N_f = 13.3N_f + 23.4$ obtained in Ref. 21) and Ref. 11), respectively.

4. Concluding Remarks

We performed computer simulations of normal grain growth in 3D by using the MPF model. For the purpose of the acceleration of computation, we applied both the APT algorithm and the parallel coding techniques to the MPF model. We have reconfirmed that the MPF is a powerful tool for simulating grain growth. Especially, the procedure described in this paper is highly efficient. As mentioned in Section 2.2, the implementation of the parallelization was quite easy. Further, the memory consumption of our procedure was 1/3 of that in Ref. 21) (Fan and Chen model with the DGR algorithm and the parallel coding techniques) even for the simulation of the normal grain growth. The difference will be larger with the introduction of anisotropy into grain boundary properties. As pointed out by Kim *et al.*,[18] the easiness of the calculating topological characteristics of grains is an advantage of MPF+APT scheme.

Aknowledgements

This study was partially supported by the Next Generation Supercomputer Project, Nanoscience Program, MEXT, Japan. It was also supported by the CREST, Japan Science and Technology Agency.

REFERENCES

1) H. V. Atkinson: Acta Metall. **36** (1988) 469–491.
2) D. Weaire and J. A. Glazier: Materials Science Forum **94–96** (1992) 27–38.
3) M. Hillert: Acta Metall. **13** (1965) 227–238.
4) J. E. Burke and D. Turnbull: Prog. Metal Phys. **3** (1952) 220–292.
5) N. P. Louat: Acta Metall. **22** (1974) 721–724.
6) D. Weaire and F. Bolton: Phys. Rev. Lett. **65** (1990) 3449–3451.
7) D. Weaire and J. P. Kermode: Phil. Mag. **B48** (1983) 245–249.
8) D. Weaire and H. Lei: Phil. Mag. Lett. **62** (1990) 427–430.
9) K. Kawasaki, T. Nagai and K. Nakashima: Phil. Mag. **B 60** (1989) 399-421.
10) C. V. Thompson, H. J. Frost and F. Spaepen: Acta Metall. **35** (1987) 887–890.
11) F. Wakai, N. Enomoto and H. Ogawa: Acta Mater. **48** (2000) 1297–1311.
12) M. P. Anderson, D. J. Srolovitz, G. S. Grest and P. S. Sahni: Acta Metall. **32** (1984) 783–791.
13) D. J. Srolovitz, M. P. Anderson, P. S. Sahni and G. S. Grest: Acta Metall. **32** (1984) 793–802.
14) D. Fan and L.-Q. Chen: Acta Mater. **45** (1997) 611–632.
15) D. Fan, C. Geng and L.-Q. Chen: Acta Mater. **45** (1997) 1115–1126.
16) A. Kazaryan, Y. Wang, D. A. Dregia and B. R. Patten: Acta Mater. **50** (2002) 2491–2502.
17) N. Ma, A. Kazaryan, D. A. Dregia and Y. Wang: Acta Mater. **50** (2002) 3869–3879.
18) S. G. Kim, D. I. Kim, W. T. Kim and Y. B. Park: Phys. Rev. **E 74** (2006) 061605-1–061605-14.
19) J. A. Warren, R. Kobayashi, A. Lobkovsky and W. C. Carter: Acta Mater. **51** (2003) 6035–6058.
20) C. E. Krill and L.-Q. Chen: Acta Mater. **50** (2002) 3057–3073.
21) Y. Suwa, Y. Saito and H. Onodera: Comput. Mater. Sci. **40** (2007) 40–50.
22) Y. Suwa, Y. Saito and H. Onodera: Scripta Mater. **55** (2006) 407–410.

23) S. Vedantam and B. S. V. Patnaik: Phys. Rev. **E 73** (2006) 016703-1–016703-8.
24) J. Gruber, N. Ma, Y. Wang, A. D. Rollett and G. S. Rohrer: Model. Simul. Mater. Sci. Eng. **14** (2006) 1189–1195.
25) I. Steinbach and F. Pezzolla: Physica **D 134** (1999) 385–393.
26) F. J. Humphreys and M. Hatherly: *Recrystallization and related annealing phenomena*, (Pergamon, Oxford. 1995).
27) S. G. Kim, W. T. Kim, T. Suzuki and M. Ode: J. Crystal Growth **261** (2004) 135–158.
28) Y. Suwa, Y. Saito and H. Onodera: Acta Mater **55** (2007) 6881–6894.
29) S. Sakamoto and F. Yonezawa: Kotai Butsuri (Solid State Physics), **24** (1989) 219–226.
30) A. A. B. Sugden and H. K. D. H. Bhadeshia: *Recent Trends in Welding Science and Technology*, ed. by S. A. David and J. M. Vitek, (ASM International, Ohio, USA, 1989) pp. 273–278.
31) D. Weaire and S. Hutzler: The Physics of Foams. Oxford, Clarendon press. 1999.
32) D. Zöllner and P. Streitenberger: Scripta Mater. **54** (2006) 1697–1702.
33) P. Streitenberger and D. Zöllner: Scripta Mater. **55** (2006) 461–464.
34) D. A. Aboav: Metallography, **5** (1970) 251–263.
35) D. Weaire and N. Rivier: Contemporary Physics **25** (1984) 59–99.